Magnetic Instruments

Patterning of Subwavelength Magnetic Fields Along a Line by Means of Spatial Spectrum: Design and Implementation

Amirhossein Hajiaghajani* and Ali Abdolali**

Bioelectromagnetics Group, Applied Electromagnetics Laboratory, School of Electrical Engineering, Iran University of Science and Technology, Tehran 1684613114, Iran
* *Student Member, IEEE*
** *Senior Member, IEEE*

Received 2 Aug 2017, revised 17 Aug 2017, accepted 20 Aug 2017, published 29 Aug 2017, current version.

Abstract—Spatial shaping of magnetic fields at low frequencies has various applications in biophysics such as magnetic drug targeting, magnetic innervation, and hyperthermia. In this letter, for a given arbitrary one-dimensional magnetic pattern, the spatial spectrum is calculated by Fourier series. It is shown that a set of regularly spaced coils realizes a controlled sinusoidal base pattern, that is, a typical spatial mode, along a target line parallel to axis of the coil array. Hence, multimode sets were employed simultaneously to synthesize the fundamental spectra of the desired pattern. In a specific mode, each coil's center and radius are specified by the corresponding spectrum, while the current is proportional to the Fourier coefficients. Every coil set was fabricated on a thin dual-layer printed circuit board and then mounted on each other. An excellent agreement between the analytical solution and experiment results was obtained using the five modes of the spectrum. The proposed setup is simple to realize, electronically reconfigurable, and allows for fast analysis.

Index Terms—Magnetic instruments, subwavelength patterning, magnetic pattern synthesis, magnetic innervation, magnetic drug targeting.

I. Introduction

Spatial patterning of magnetic (H) fields is referred to as forming fields as a function of coordinates in space. Although near-field patterning of high-frequency electromagnetic fields (from hundreds of megahertz to gigahertz) usually has been realized by phase array antennas, such a technique cannot be used at low frequencies because every two different observation points have the same phase [Balanis 2012]. The arbitrary subwavelength patterning still remains a challenging subject among various applications in biophysics, such as magnetic hyperthermia [Hergt 2004, Laurent 2011, Bellizzi 2015], magnetic drug targeting through a blood vessel [Cherry 2010, Tehrani 2014, Hajiaghajani 2017], magnetic innervation and neuron rehabilitation [Roth 1990, Ruohonen 1996, Davey 2000, Haan 2014], and wireless power transfer for implanted devices [Jian 2016, Sun 2016]. Additionally, the technology is essential for low-frequency imaging [Lee 1993], and biasing of reconfigurable and graphene-based structures [Sung 2004, Castro 2007, Xiao 2007].

In recent research, coil arrays have played a considerable role in focusing of magnetic fields [Gao 2015, Choi 2016]. However, the analytical approach to find the coil currents is often an unwieldy and time-taking procedure [Markley 2008].

This letter proposes a fast technique for controlling the spatial pattern of magnetic fields. We consider the spatial spectrum of a desired one-dimensional (1-D) pattern and discuss the fabrication and placement of a coil array in order to realize each spectrum separately. Simultaneous usage of these arrays produces multiple spatial spectra. The arrays are fed by currents whose values are found by using the Fourier coefficients. The similarity between the desired pattern and the realized profile is quantified and employed to enhance the synthesis accuracy. Applicability of this method is validated by both simulation and experimental implementation. The setup includes five sets of coils mounted above each other. The desired 1-D sample pattern is synthesized at a distance of 1 cm from the coils.

Corresponding author: Ali Abdolali (e-mail: abdolali@iust.ac.ir).
Digital Object Identifier 10.1109/LMAG.2017.2746065

II. Spatial Patterns in Terms of the Fourier Series

In this section, $f(x)$ is assigned to the arbitrary H field pattern and is considered to be synthesized along the x-axis. Assuming that $f(x)$ is well behaved on the domain set $[0, L]$, it can be expanded by the Fourier series as follows [Kreyszig 2011]:

$$f(x) = \frac{1}{2} a_0 + \sum_{n=1}^{\infty} \left\{ a_n \cos\left(\frac{2\pi n x}{L}\right) + b_n \sin\left(\frac{2\pi n x}{L}\right) \right\} \quad \text{(1a)}$$

where the coefficients are calculated by

$$a_n = \frac{2}{L} \int_0^L f(x) \cos\left(\frac{2\pi n x}{L}\right) dx, \quad n = 0, 1, 2, \ldots \quad \text{(1b)}$$

$$b_n = \frac{2}{L} \int_0^L f(x) \sin\left(\frac{2\pi n x}{L}\right) dx, \quad n = 1, 2, 3, \ldots. \quad \text{(1c)}$$

In practical and engineering subjects, the series contains finite modes (n varies from 0 to N). Throughout this letter, we refer to the Fourier reconstruction of the Nth order by $\tilde{f}$. We aim to realize the base sinusoidal profiles by using coil arrays and finally synthesize $\tilde{f}$ on set $[0, L]$.

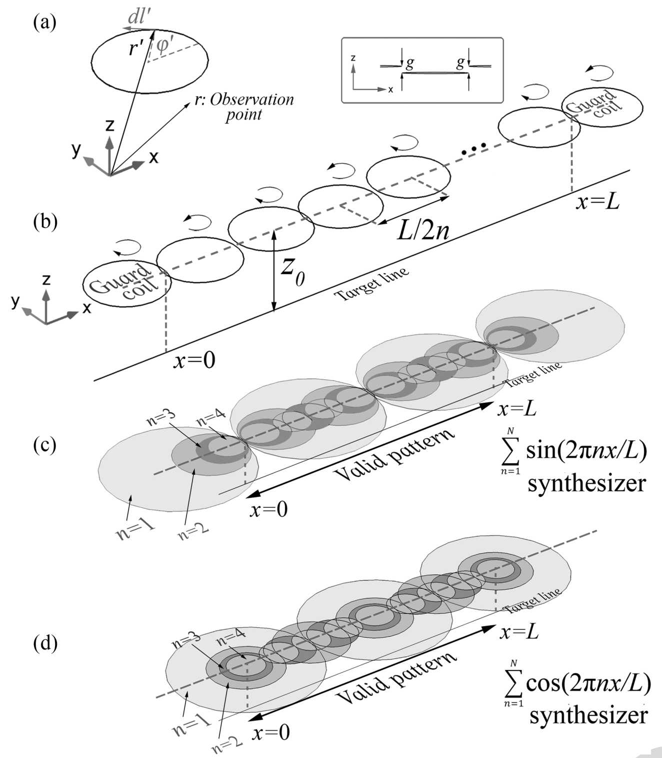

Fig. 1. (a) Circular curve's geometry. (b) Typical sets of coils whose magnetic pattern is greatly similar to a sine function. (c), (d) Combination of stacked sets to respectively realize odd (sine) and even (cosine) sentences of the Fourier representation of the desired magnetic field pattern.

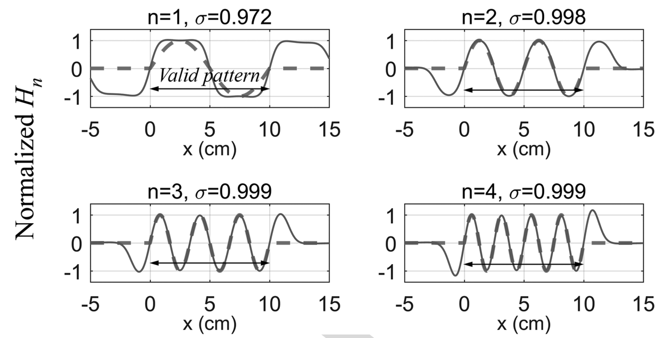

Fig. 2. Synthesis of various sine modes along a line placed 1 cm beneath the coils. Solid and dashed lines indicate the produced field and the corresponding sinusoidal mode, respectively. Patterns are valid between [0, L = 10 cm]. The correlation values (between the sine function and the realized field in valid intervals) are marked. The distortion only in the first mode is made, since z_0 is lower than R_1. Although the distortion will affect the accuracy of the synthesis, it is acceptable due to its high correlation. We accept marginally lower accuracy of the first mode at the expense of not losing the field's amplitude in higher modes. It is shown the guard coils produce additional sine lobes out of the valid region and enhance the correlation within the valid interval.

III. Realization of the Base Functions

In the previous section, $\tilde{f}$ was expanded in terms of sinusoidal bases as a function of x. Here, we aim to realize the sentences appeared in (1a) by connecting each sinusoidal mode to an array of subwavelength coils. The magnetic quasi-static fields produced by a circular coil (with equiphasic approximation and the wavenumber much lower than unity) of radius R which runs current of I (phasor notation) is obtained by [Griffiths 1999]

$$\vec{H}\ (x, y, z) = \frac{I}{4\pi}\int_c \frac{\overrightarrow{d\ell'} \times \left(\vec{r} - \overrightarrow{r'}\right)}{\left|\vec{r} - \overrightarrow{r'}\right|^3} \tag{2}$$

where $\vec{r}$ and $\overrightarrow{r'}$, respectively, represent the vectors of observation point and point on the circular curve c [see Fig. 1(a)]. Assuming the coil is centered at the origin, the produced H_z (z component of the magnetic field, i.e., the dominant component) is obtained by substituting the observation point along the target line $y = z - z_0 = 0$ into (2)

$$H_z\ (x, 0, z_0) = \frac{I}{4\pi}\int_0^{2\pi} \frac{R^2 - Rx\ \cos\varphi'}{(x^2 + z_0^2 + R^2 - 2Rx\ \cos\varphi')^{1.5}} d\varphi'. \tag{3}$$

H_z peaks at $x = 0$ (beneath the coil's center). If $z_0 \geq R$, the analytical solution acquired by discretization of this elliptic integral is noticeably similar to one sine lobe with a spatial wavelength of $4R$. The similarity is still established even if z_0 is marginally smaller than R. To realize a single-mode sinusoidal pattern function $\sin(2\pi nx/L)$ on the target line $y = z - z_0 = 0$ within $0 < x < L$, an array of $2n + 2$ coils, all with the radius of $R_n (= \frac{L}{4n}\ )$ and centered at $((2i\ -\ 1)R_n, 0, \frac{g}{2}(-1)^i), i = 0, 1, \ldots, 2n + 1$ is proposed where g is the very minute distance between two adjacent coils in the z-direction. Axis of the coil array is parallel to the target line. Coils lie on the z-plane and run same current (I_n) but in the opposed direction relative to the adjacent coil, in order to interpret positive and negative peaks of the sine function [see Fig. 1(b)]. The two guard coils (peripheral coils corresponding to $i = 0$ and $2n + 1$, which are placed out of the set [0, L]) are essential to form a clear sinusoidal spatial shape within the set.

Under this combination, the resultant perpendicular magnetic field of the nth mode is obtained by the following series:

$$H_n = \sum_{i=0}^{2n+1} (-1)^{i+1} H_z \left(x - (2i - 1)\, R_n,\ 0,\ z_0 - \frac{g}{2}(-1)^i\right) \tag{4}$$

Substituting (3) into (4) reduces to a pattern of magnetic field, which shows remarkable likeness to function $\sin(2\pi nx/L)$ within [0, L]. To show this similarity for a typical mode n, the normalized cross-correlation criterion defined by

$$\sigma\,(A, B)\ = \frac{\int_{-L}^{L}\left(A - \bar{A}\right)\left(B - \bar{B}\right)\, dx}{\sqrt{\left(\int_{-L}^{L}\left(A - \bar{A}\right)^2 dx\right)\left(\int_{-L}^{L}\left(B - \bar{B}\right)^2 dx\right)}} \tag{5}$$

is employed, where $\bar{X} = \frac{1}{2L}\ \int_{-L}^{L} X dx$. As σ approaches to 1, the similarity between functions A and B increases. The sinusoidal pattern of H_n becomes distorted when z_0 is much lower than R_n. On the other hand, the amplitude of the magnetic field reduces dramatically by increasing z_0. According to (3), this becomes important especially for higher modes, where R becomes smaller.

The first four modes of H_n are depicted in Fig. 2 for $z_0 = L/10$. At such distance we attain both 1) an acceptable correlation between H_n and $\sin(2\pi nx/L)$ with $\sigma > 0.95$ and 2) lower amplitude loss. Nonetheless regarding the application, one can adjust the distance marginally in order to reach greater synthesis accuracy or lower amplitude loss.

Using the proposed array, a sinusoidal magnetic field pattern was realized. We aim to find I_n, such that the resultant H_n (as a function of x, n, and I_n) becomes equal to a typical sine function of (1a). To this end, (3) is substituted into (4) to derive

$$I_n \times \sum_{i=0}^{2n+1} \frac{(-1)^{i+1}}{4\pi} \int_0^{2\pi} \frac{R_n^2 - R_n(x - x_i)\cos\varphi'}{\left((x - x_i)^2 + z_i^2 + R_n^2 - 2R_n(x - x_i)\cos\varphi'\right)^{1.5}}\, d\varphi' = b_n \sin\left(\frac{2\pi n x}{L}\right) \quad (6)$$

where x_i and z_i ($\cong z_0$) are respectively the x and z components of center of the ith coil in the array [a_n and b_n are known by (1)]. The high correlation values for various modes show that the left-hand side of (6) behaves like the sine function on the right-hand side; thus, the resultant I_n is proportional to b_n. The simultaneous usage of multiple sine modes (i.e., summation of multiple modes of H_n) realizes sine sentences of (1a). Fig. 1(c) depicts the general setup for synthesizing the sine modes.

Similarly, the discussed method holds true for the cosine sentences of (1a). To this end, centers of the coils of each mode must be shifted toward the $+x$ direction by R_n. Therefore, these coils are centered at $(2iR_n, 0, \frac{g}{2}(-1)^i)$, $i = 0, 1, \ldots, 2n$ as shown in Fig. 1(d). In this case, the resultant H_n realizes $a_n \cos(\frac{2\pi n x}{L})$ and currents are found by an analogous approach. Additionally, for $a_0 \neq 0$, a long rectangular coil with a length of L (in the x-direction) and small width (e.g., 4 cm in the y-direction) centered at $(L/2,\ 0,\ z_0)$ would produce a constant magnetic pattern. A detailed analysis of radiation from an oblong rectangular coil is available in Jackson [1999].

It was shown that coefficients of the Fourier series (denoted by c_n, which is a_n or b_n) are linearly proportional to the currents that ran on their corresponding modes. In order to adjust the amplitude of the induced magnetic field by the entire setup (H_{tot}), first, the amount of all currents should be scaled (multiplied by α_0) according to the magnitude level of the required field. Second, the coil sets are stacked and each set is distanced by z_n from the target line. In order to compensate the effect of small vertical displacement, currents of each mode should be modified anisotropically (multiplied by β_n). Accordingly, current of coils in the nth set is obtained by

$$I_n = \alpha_0\, \beta_n c_n, \quad c_n = a_n \text{ or } b_n. \quad (7a)$$

The exact value of $(\alpha_0 \beta_n)$ can be obtained from (6). As a simple rule of thumb, regarding the coil radius, β_n can be found separately by substituting a peak's coordinate of H_n (e.g., $(L/4n, 0, 0)$) in (6). Therefore

$$\beta_n \cong \left(\frac{{R_n}^2 + z_n^2}{{R_n}^2 + z_0^2}\right)^{1.5} \quad (7b)$$

which is the ratio of the current of displaced set at z_n to the current of fixed set at z_0. It is observed that for larger coils (with lower orders of the Fourier spectrum), these vertical displacements do not make noticeable effect and $\beta_n \cong 1$.

It should be noted that coils can be fed by nonsinusoidal waveforms (e.g., with a frequency modulation in imaging, tomography, etc.) as long as the bandwidth of the current signals lies within the subwavelength frequency span.

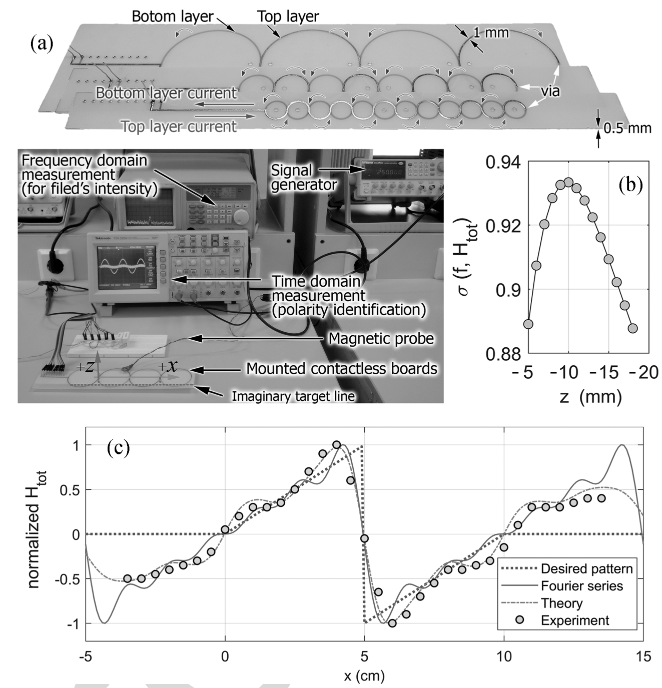

Fig. 3. Synthesis of a high gradient triangular-shaped sample pattern. (a) Fabricated coils on PCBs and the measurement setup. To ease the measurement, the setup and spacer were rotated. The gridded spacer is not shown. (b) Correlation value reflects the optimum distance between the target line and the setup ($N = 5$). To attain the highest synthesis accuracy, the bottom frontier of the setup must be placed 1 cm ($L/10$) above the target line. (c) Results of simulation and measurement for magnetic fields for $N = 5$ on a line 1 cm beneath the coils. The solution is only valid between [0, $L = 10$ cm]. Under this situation, the peak of 5 A/m at 250 kHz was measured by the probe.

IV. Setup Fabrication and Validation

Here, we discuss the design procedure of the pattern synthesizer setup. Each mode was fabricated on a dual-layer printed circuit board (PCB) with the thickness of 0.5 mm. Top and bottom layers of each board were connected at one point by a via in order to behave like contactless loops [see Fig. 3(a)]. Because of series coils in each set, the number of sources is dramatically less than the number of coils; this is recognized as a certain advantage of this device. Given a sample triangular pattern, the reconstructed function by the Fourier series ($\tilde{f}$) was calculated [as shown in Fig. 3(c)]. In order to eliminate H_{tot} at $x < 0$ and $x > L$, one can expand the spatial period L, define a new f with zero fields around the old pattern, and then follow the synthesis procedure.

The calculation of correlation between f and H_{tot} for five coil sets shows that the most accurate pattern is synthesized at $z_0 = 0.1\,L$ (see Fig. 3(b); same result was obtained for various values of N and L). In addition, the correlation values between f, $\tilde{f}$, and H_{tot} along the target line $y = z + 1\,\text{cm} = 0$ for various Fourier orders (N) are compared in Table 1.

As expected, it is found that to reach a greater correlation, one may employ higher order Fourier modes. We chose $N = 5$ and mounted the five contactless boards on each other. This subwavelength structure is able to work from dc to hundreds of MHz; however, we fed layers by in-phase currents at 250 kHz (a common frequency for modern hyperthermia [Golovin 2015]). The currents were found based on the

Table 1. Effect of number of the coil sets in the setup (N) on σ. Functions and fields are truncated for $x = [0,\ L = 10$ cm]. Target line was placed 1 cm beneath the setup.

N	$\sigma(f, \tilde{f})$	$\sigma(f, H_{\text{tot}})$
4	0.9307	0.9284
5	0.9438	0.9333
6	0.9528	0.9331

Table 2. Calculation of the currents applied to each layer for $N = 5$, $L = 10$ cm, $z_0 = -1$ cm, and $\alpha_0 = 0.44$.

n	R_n (mm)	z_n (mm)	b_n (A/m)	β_n	I_n (mA)
1	25	–12	0.636	1.09	306
2	12.5	–11.5	–0.318	1.19	–167
3	8.33	–11	0.212	1.19	111
4	6.25	–10.5	–0.158	1.11	–77
5	5	–10	0.126	1.00	56

Fourier coefficients, distance of the target line, coil radius, and scaling coefficients, and are represented in Table 2. Using a resistive current divider circuit, expected currents were imposed with a tolerance of ± 12 mA. The experimental setup is shown in Fig. 3(a).

A small multiturn loop with a radius of 3 mm and connected to a spectrum analyzer was used as a magnetic probe to measure the near field's amplitude. Also, the probe was connected to an oscilloscope to identify the field's polarity. The target line was structured by a polystyrene planar spacer with the thickness of 1 cm and was gridded. The probe was positioned centered over the target line, and manually scanned over the axis of the coil arrays in 5 mm steps. With a good dynamic range of 41 dB (from the pattern's null to peak), the desired and measured patterns were in a very good agreement, with the correlation value of up to 0.92.

Since the proposed scheme is free of magnetizable parts (e.g., iron cores, ferrites, etc.), no magnetic saturations occur. Therefore, the amplitude of the pattern can be maximized regarding the maximum tolerable temperature of the boards. The amplitude can be increased by using cooling systems and particular PCB substrates.

V. Conclusion

A new approach to design and fabrication of a magnetic pattern synthesizer was proposed and validated by simulation and experiment, as well. Since the conventional patterning techniques such as phase arrays cannot be generalized to subwavelength instruments, the design procedure presented in this letter, for the first time, follows an analytical straightforward approach by rewriting the arbitrary linear pattern in terms of Fourier spatial spectra. A coil array was introduced to realize each spectrum. In order to enhance the pattern's resolution, more Fourier modes and hence more sets of coils should be employed. The magnetic fields were spatially shaped from dc to hundreds of megahertz. The setup is easy to fabricate on PCBs, requires a significantly low number of current sources, and free of unwieldy current calculation. The proposed technique will find applications in magnetic particle imaging, tomography, magnetic drug targeting, and magnetic field scanners by sweeping the setup and record induced fields.

REFERENCES

Balanis C A (2012), *Advanced Engineering Electromagnetics*, 2nd ed. Hoboken, NJ, USA: Wiley. [Online]. Available: http://www.wiley.com/WileyCDA/WileyTitle/productCd-EHEP002059.html

Bellizzi G, Bucci O M (2015), "Blind focusing of electromagnetic fields in hyperthermia exploiting target contrast variations," *IEEE Trans. Biomed. Eng.*, vol. 62, pp. 208–217, doi: 10.1109/TBME.2014.2344711.

Castro E V, Novoselov K S, Morozov S V, Peres N M R, Dos Santos J M B L, Nilsson J, Guinea F, Geim A K, Neto A H C (2007), "Biased bilayer graphene: Semiconductor with a gap tunable by the electric field effect," *Phys. Rev. Lett.*, vol. 99, 218602, doi: 10.1103/PhysRevLett.99.216802.

Cherry E M, Maxim P G, Eaton J K (2010), "Particle size, magnetic field, and blood velocity effects on particle retention in magnetic drug targeting," *Med. Phys.*, vol. 37, pp. 175–182, doi: 10.1118/1.3271344.

Choi B H, Kim J H, Cheon J P, Rim C T, Jun P, Rim C T (2016), "Synthesized magnetic field focusing using a current-controlled coil array," *IEEE Magn. Lett.*, vol. 7, 6501504, doi: 10.1109/LMAG.2016.2520903.

Davey K, Epstein C M (2000), "Magnetic stimulation coil and circuit design," *IEEE Trans. Biomed. Eng.*, vol. 47, pp. 1493–1499, doi: 10.1109/10.880101.

Gao F, Zhang F, Wakatsuchi H, Sievenpiper D F (2015), "Synthesis and design of programmable subwavelength coil array for near-field manipulation," *IEEE Trans. Microw. Theory Techn.*, vol. 63, pp. 2971–2982, doi: 10.1109/TMTT.2015.2450711.

Golovin Y I, Gribanovsky S L, Golovin D Y, Klyachko N L, Majouga A G, Master A M, Sokolsky M, Kabanov A V (2015), "Towards nanomedicines of the future: Remote magneto-mechanical actuation of nanomedicines by alternating magnetic fields," *J. Control. Release*, vol. 219, pp. 43–60, doi: 10.1016/j.jconrel.2015.09.038.

Griffiths D J (1999), *Introduction to Electrodynamics*. Englewood Cliffs, NJ, USA: Prentice-Hall.

Haan N, Song B (2014), "Therapeutic application of electric fields in the injured nervous system," *Adv. Wound Care*, vol. 3, pp. 156–165, doi: 10.1089/wound.2013.0450.

Hajiaghajani A, Hashemi S, Abdolali A (2017), "Adaptable setups for magnetic drug targeting in human muscular arteries: Design and implementation," *J. Magn. Magn. Mater.*, vol. 438, pp. 173–180, doi: 10.1016/j.jmmm.2017.04.058.

Hergt R, Hiergeist R, Hilger I, Kaiser W A, Lapatnikov Y, Margel S, Richter U (2004), "Maghemite nanoparticles with very high AC-losses for application in RF-magnetic hyperthermia," *J. Magn. Magn. Mater.*, vol. 270 pp. 345–357, doi: 10.1016/j.jmmm.2003.09.001.

Jackson J D (1999), *Classical Electrodynamics*. Hoboken, NJ, USA: Wiley. [Online]. Available: http://www.wiley.com/WileyCDA/WileyTitle/productCd-047130932X.html

Jian J, Stana M, Stanaćević M (2016), "Adaptive transmitting coil array for optimal power transfer in deeply implanted medical devices," in *Proc. IEEE Int. Symp. Circuits Syst.*, pp. 2030–2033, doi: 10.1109/ISCAS.2016.7538976.

Kreyszig E (2011), *Advanced Engineering Mathematics*, 10th ed. Hoboken, NJ, USA: Wiley. [Online]. Available: http://www.wiley.com/WileyCDA/WileyTitle/productCd-EHEP001850.html

Laurent S, Dutz S, Häfeli U O, Mahmoudi M (2011), "Magnetic fluid hyperthermia: Focus on superparamagnetic iron oxide nanoparticles," *Adv. Colloid Interface Sci.*, vol. 166, pp. 8–23, doi: 10.1016/j.cis.2011.04.003.

Lee K H, Xie G (1993), "A new approach to imaging with low-frequency electromagnetic fields," *Geophysics*, vol. 58, pp. 780–796, doi: 10.1190/1.1443464.

Markley L, Wong A M H, Wang Y, Eleftheriades G V (2008), "Spatially shifted beam approach to subwavelength focusing," *Phys. Rev. Lett.*, vol. 101, 113901, doi: 10.1103/PhysRevLett.101.113901.

Roth B J, Basser P J (1990), "A model of the stimulation of a nerve fiber by electromagnetic induction," *IEEE Trans. Biomed. Eng.*, vol. 37, pp. 588–597, doi: 10.1109/10.55662.

Ruohonen J, Panizza M, Nilsson J, Ravazzani P, Grandori F, Tognola G (1996), "Transverse-field activation mechanism in magnetic stimulation of peripheral nerves," *Electroencephalogr. Clin. Neurophysiol.*, vol. 101, pp. 167–174, doi: 10.1016/0924-980X(95)00237-F.

Sun J-S, Pan G P, Hsu C-Y, Li T-L (2016), "Study of the smart contactless charging platform with coil array," in *Proc. IEEE Int. Symp. Radio-Freq. Integr. Technol.*, pp. 1–4, doi: 10.1109/RFIT.2016.7578125.

Sung Y J, Jang T U, Kim Y S (2004), "A reconfigurable microstrip antenna for switchable polarization," *IEEE Microw. Wireless Components Lett.*, vol. 14, pp. 534–536, doi: 10.1109/LMWC.2004.837061.

Tehrani M D, Kim M O, Yoon J (2014), "A novel electromagnetic actuation system for magnetic nanoparticle guidance in blood vessels," *IEEE Trans. Magn.*, vol. 50, 5100412, doi: 10.1109/TMAG.2014.2307271.

Xiao D, Yao W, Niu Q (2007), "Valley-contrasting physics in graphene: Magnetic moment and topological transport," *Phys. Rev. Lett.*, vol. 99, 236809, doi: 10.1103/PhysRevLett.99.236809.